Journal of Porous Materials (2023) 30:493–505
https://doi.org/10.1007/s10934-022-01359-2

A green route to synthesize HZSM-5 zeolites for the coreaction of n-heptane and methanol to light olefins

Rui Feng[1] · Bao Liu[1] · Xiaoyan Hu[1] · Xinlong Yan[1] · Min Zhou[1]

Accepted: 24 September 2022 / Published online: 6 October 2022

Abstract
H-form HZSM-5 zeolites are important industrial materials. However, their direct synthesis remains challenging since they have to be synthesized in the presence of a Na alkaline solvent. Herein, we report that ammonia hydroxide can serve as an alkaline source for the direct synthesis of HZSM-5 zeolites by steam-assisted crystallization (SAC) and dynamic agitation crystallization (DAC). We demonstrated that the mass transfer of silicon and aluminum sources is crucial for the crystallization process; therefore, the crystallization rate of HZSM-5 by DAC is considerably faster than that by SAC. The catalytic performances of the coreaction of n-heptane and methanol show that the cracking products of n-heptane participate in the dual-cycle reactions of methanol, leading to an enhanced yield of light olefins but a reduced catalyst lifetime because of an accelerated coking rate. This study contributes a green route to the synthesis of HZSM-5 zeolites and provides insight for improving the yield of light olefins.

Keywords H-form ZSM-5 · Steam-assisted crystallization · Dynamic agitation crystallization · Catalytic cracking · Methanol to olefins

1 Introduction

Light olefins (ethylene, propylene, and butylene) are the primary building blocks for modern chemical industries and are traditionally produced by the thermal/catalytic cracking of petroleum sources [1, 2]. Recently, methanol or dimethyl ether, which can be produced from renewable biomass or coal, has been increasingly used as a raw material for the production of light olefins [3]. With the increasing consumption of synthetic materials of polymers and fine chemicals, the demand for raw materials for light olefins has rapidly increased [3–5]. ZSM-5 zeolites, in the catalytic cracking and methanol to olefins (MTO) processes, are dominant industrial catalysts, owing to their high selectivity for light olefins and relatively long-running cycle, which has attracted extensive attention and has been a hot topic for several years [6, 7].

In general, methanol conversion over a ZSM-5 catalyst will produce a proportion of aliphatic-rich C_5/C_6/C_7 + byproducts, which can be used as a recycling stream to improve propylene selectivity [8]. In addition, the cracking of hydrocarbons is an endothermic reaction, while methanol conversion is an exothermic reaction [9]. Considering that methanol and aliphatic hydrocarbons can be converted to light olefins, the coreaction of two feedings over ZSM-5 catalysts should be meaningful [10, 11]. For instance, Ebadzadeh et al. [11] recently studied the coreaction of methanol and a C_4–C_5 olefin mixture over the HZSM-5 catalyst and observed that the cofeeding of the C_4–C_5 olefin mixture with methanol could remarkably enhance propylene selectivity by controlling the operating conditions.

The ZSM-5 zeolite has a unique three-dimensional porous structure of a straight channel intersected with a sinusoidal channel, which can enhance the shape selectivity for propylene molecules [12, 13]. However, ZSM-5 zeolites are traditionally prepared in a Na^+-alkaline solvent and hydrothermally crystallized at approximately 170 °C for over 2 days [14]. The Na^+ counter ions can balance the charge on the aluminosilicate ions; therefore, a Na-form ZSM-5 zeolite is first obtained after the crystallization process. NH_4^+-ion exchange is a necessary intermediate step

✉ Rui Feng
fengrui@cumt.edu.cn; feng2007115@163.com

[1] School of Chemical Engineering and Technology, China University of Mining and Technology, Xuzhou 221116, Jiangsu, China

Scheme 1 A diagram showing HZSM-5 synthesis by steam-assisted crystallization (SAC).

to transform the Na-form ZSM-5 zeolite to a NH_4^+-form zeolite, and finally to an H-form HZSM-5 zeolite by calcination [15, 16]. In addition, multiple ion exchanges and drying or calcination steps are typically required to increase the sodium content to industrial application standards. Therefore, whether during the one-pot hydrothermal crystallization or the subsequent ion-exchange process, water pollution and high energy consumption are unavoidable [17, 18]. Recently, several studies have tried to use metal-free mineralizers, such as ammonia and fluoride, instead of the traditional sodium alkaline for the synthesis of Na-free zeolites [15, 16]. For instance, Bibby et al. [15] reported the first use of an ammonium hydroxide (NH_4OH) system to synthesize ZSM-5 and ZSM-11 zeolites, and an H-form ZSM-5 zeolite was directly obtained Wu et al. [16] reported a solvent-free route to directly synthesize an H-type MFI zeolite with NH_4F; however, a high proportion of parent ZSM-5 was used for the crystallization, and the residual F in the product probably limited its application.

Previously, we directly synthesized H-form ZSM-5 zeolites using a static hydrothermal crystallization method with ammonia hydroxide as an alkaline source [19, 20]. In addition, a dry-gel conversion method was adopted for the direct one-pot synthesis of Na-type Fe-ZSM-5 zeolites, which still required an ion-exchange step [21]. Therefore, here, we directly synthesized H-form ZSM-5 zeolites using ammonia as a mineralizer by steam-assisted crystallization (SAC) and dynamic agitation crystallization (DAC). It can avoid the repeated ion-exchange process in traditional sodium alkaline for the synthesis of Na-free zeolites. In particular, cheap commercial solid fumed silica and pseudoboehmite were used as raw materials instead of expensive metal organic alkoxides. In addition, it was found that the coreaction of n-heptane and methanol over the HZSM-5 catalyst improved the cracking of n-heptane, which exhibited high selectivity for light olefins but a faster deactivation rate, compared with that from separate feeds. These catalysts were used to investigate the coreaction of methanol and n-heptane. We expect this study to provide a novel, efficient, and ecofriendly strategy for the one-pot synthesis of H-form ZSM-5 zeolites.

2 Experimental section

2.1 Materials

Fumed silica (nano-SiO_2, approximately 20 nm) was purchased from Qinghe Andi Metal Materials Co. Pseudoboehmite (PB) with 71.90 wt% of Al_2O_3 on a dry basis was provided by Hua Xin Powder Co. Ltd. Ammonium hydroxide ($NH_3{\cdot}H_2O$, 25–28 wt%); tetrapropyl ammonium bromide [TPABr, analytical reagent (AR)]; and tetrapropyl ammonium hydroxide (TPAOH, 25 wt% aqueous solution) were purchased from Sinopharm Chemical Reagent Co., Ltd. and used without further purification.

2.2 Zeolite synthesis

The HZSM-5 zeolites were synthesized by SAC using ammonia hydroxide as a mineralizer. Conventionally, fumed silica, PB, and TPAOH were mixed in a mortar and ground for approximately 20 min, and the mixture was transferred into an autoclave reactor with ammonia hydroxide solution at the bottom, as shown in Scheme 1. Crystallization was performed in an oven at 180 °C for a certain time. The solid product was removed from the autoclave and dried at 110 °C overnight. The H-form ZSM-5 zeolites were obtained after simple calcination at 550 °C for 4 h. The type and composition of the raw materials were changed to investigate the effect of the synthesis conditions on crystallization.

For comparison, DAC was employed for the direct synthesis of HZSM-5 zeolites. Typically, fumed silica, PB, TPAOH, and ammonia hydroxide were mixed at a chemical composition of 100 SiO_2:1.0 Al_2O_3:5.5 TPAOH:400 $NH_3{\cdot}H_2O$:6000 H_2O. The one-pot mixture was stirred at room temperature for 10 min and transferred into the autoclave reactor. The crystallization was conducted in an oil bathing pot at 180 °C for a certain time with stirring. The HZSM-5 zeolites were finally obtained after filtration, drying, and calcination at 550 °C for 4 h.

2.3 Characterization

X-ray diffraction (XRD) was performed on a Bruker D8 Advance diffractometer with CuK-Alpha1 radiation (0.15406 nm) over a 2θ range of 5°–75°, with operating parameters of 40 kV and 30 mA and a scanning speed of 0.02°/s. Scanning electron microscopy (SEM) images were recorded on a Quanta 250 instrument. Fourier transform infrared (FT-IR) spectroscopy was conducted on a Nicolet iS5 (Nicolet Instrument, Thermo Company, USA) instrument. Low-temperature N_2 sorption was performed at − 196 °C on a Micromeritics Tristar 3000, and the sample was pretreated at 350 °C and subjected to vacuum pressure for 4 h to remove any physically adsorbed moisture prior to the measurement. Thereafter, ^{27}Al and ^{29}Si magic-angle spinning nuclear magnetic resonance (MAS NMR) were measured using an Agilent 600 DD2 spectrometer (Agilent, USA, magnetic field strength 14. %) at resonance frequency of 199.13 MHz. The acidity of the samples was detected by temperature-programed desorption of ammonia (NH_3-TPD) on a Quanta Chrome ChemStar™ instrument. Thermogravimetric analysis (TGA) was performed on the spent catalysts with a Netzch STA449F5 analyzer.

2.4 Catalytic reaction tests

The HZSM-5 catalysts were obtained after tablet pressing and screening with sizes of 40–60 mesh. The catalytic performance of the catalysts was conducted in a fixed bed reactor with an inner diameter of 6 mm. A quartz tubular reactor with 0.10 g of the catalyst inside was placed in the flat-temperature zone with programed heating to 600 °C for 0.5 h as a pretreatment. N-heptane, methanol, or a mixture of these was injected into the reactor using a microplunger pump under argon carrier gas at a flow rate of 50 mL/min. The reaction was performed at atmospheric pressure within a temperature range of 430 – 590 °C at an interval of 40 °C. The reaction products were analyzed using an online gas chromatograph (GC 2014 C, Shimadzu GC), equipped with a TG-Bong Q column, thermal conductivity detector, and flame ionization detector. The mass balance was carefully controlled with an average error within 4%.

3 Results and discussion

3.1 SAC and textural properties

The crystallization of zeolites is closely related to the chemical compositions of the synthetic raw materials. To reveal the SAC evolution, aluminosilicate intermediates under different synthesis conditions were examined by XRD and FT-IR, and the results are displayed in Fig. 1. As shown in Fig. 1a, five characteristic diffraction peaks at 2θ = 8.0, 8.9, 23.2, 24.0, and 24.5° were observed, which corresponded to the (101), (200), (332), (051), and (303) planes of the MFI framework, respectively (JCPSD no. 44 - 0003) [22–24]. This showed that with an increase in the usage of ammonia hydroxide, the characteristic diffraction peaks of the MFI phase appeared, and their intensity increased, indicating that ammonia hydroxide is a prerequisite alkaline source for the formation of ZSM-5 zeolites. This correlated with the IR results shown in Fig. 1c, where the bands at 450, 547, and 1220 cm^{-1} in the FT-IR spectra were ascribed to the internal vibrations of SiO_4 and AlO_4 tetrahedra, vibration of the double five-membered ring of the MFI structure, and external asymmetric stretching bonds of T–*O*–T, respectively [25, 26]. This result confirmed the generation of the ZSM-5 phase. During the SAC, the sign of the ZSM-5 zeolite became evident when

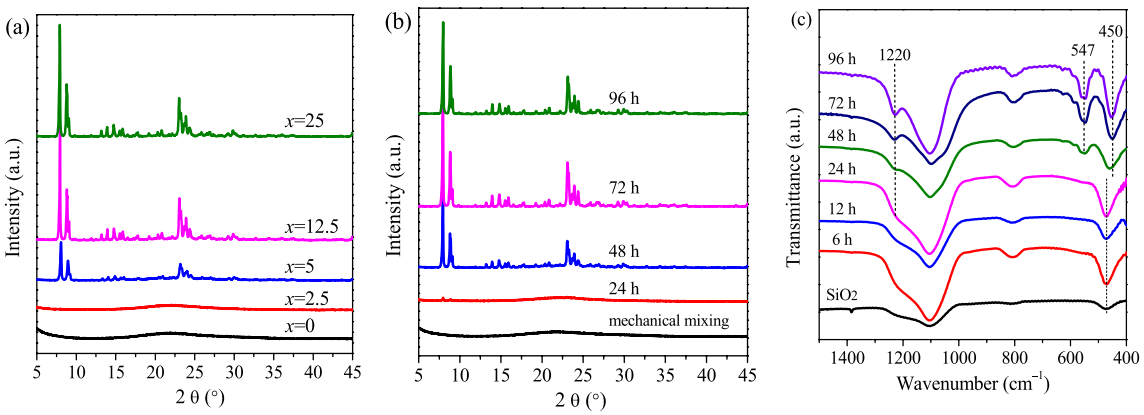

Fig. 1 **a** X-ray diffraction (XRD) patterns of samples that were crystallized for 72 h by varying the $NH_3{\cdot}H_2O$ amount with the synthesis compositions of 100 SiO_2:1.0 Al_2O_3:5.5 TPAOH:***x*** $NH_3{\cdot}H_2O$. XRD patterns **b** and Fourier transform infrared (FT-IR) spectra **c** of samples crystallized for different durations with synthesis compositions of 100 SiO_2:1.0 Al_2O_3:5.5 TPAOH:25 $NH_3{\cdot}H_2O$.

the crystallization proceeded to 48 h (Fig. 1b and c); it was relatively slower than conventional hydrothermal crystallization [20, 27].

This solid-state crystallization evolution was further characterized by SEM, as shown in Fig. 2. The fumed silica was loose unconsolidated aggregates with an average size of ~ 20 nm (Fig. 2a, b and S2). After crystallization for 24 h, nanocrystals of ZSM-5 zeolites were observed, while the majority of the fumed silica nanoparticles became big amorphous species (Fig. 2c). This was consistent with the XRD results shown in Fig. 1b and c where the sign of ZSM-5 zeolite was observed. The sample crystallized for 48 h exhibited an aggregate morphology comprising crosslinked hexagonal crystals (Fig. 2d). The crystals were relatively uniform with a size of approximately 1.5 μm along the c-axis direction of the ZSM-5 zeolite. However, they were still interbedded with amorphous aluminosilicates (Fig. 2e). The sample crystallized for 72 h became a big crosslinked hexagonal prismy structure with small amounts of amorphous species on its external surface (Fig. 2f). The crystal had a size of over 10 μm, and its surface comprised several steps. It appeared that the growth process of this solid-state crystallization followed the defect-step growth mechanism. The amorphous aluminosilicate was continually attached to the crystal surface and gradually transformed into a high crystallized step, which can be verified from the fragments in the crystalline fractures, as shown in Fig. 2 g and i.

3.2 DAC and textural properties

The effects of the synthetic raw materials on the crystallization rates were investigated, and the results are shown in Fig. 3 and S1. Fumed silica was used as a silicon source, but other raw materials were changed. When PB and ZSM-5 seed were used as the aluminum source and structure-directing agent, respectively, the crystallization was extremely slow because of the low migration rate of silicon aluminum species in a solid-state system [28]. When PB was replaced by aluminum nitrate and/or the ZSM-5 seed was replaced by tetrapropylammonium ions (TPAOH or TPABr), the crystallization is accelerated because the dispersion and mixing became even. This indicated that the mechanical mixing at a molecular level by solid-state grinding and changing the synthetic raw materials was significant for the rapid crystallization of ZSM-5 zeolites.

To verify the effects of the migration rates of the synthetic raw materials, DAC was employed to synthesize ZSM-5 zeolites in a hydrothermal autoclave with liquid-phase stirring. The crystallization rate was accelerated during the DAC process even if solid fumed silica and PB were used as raw

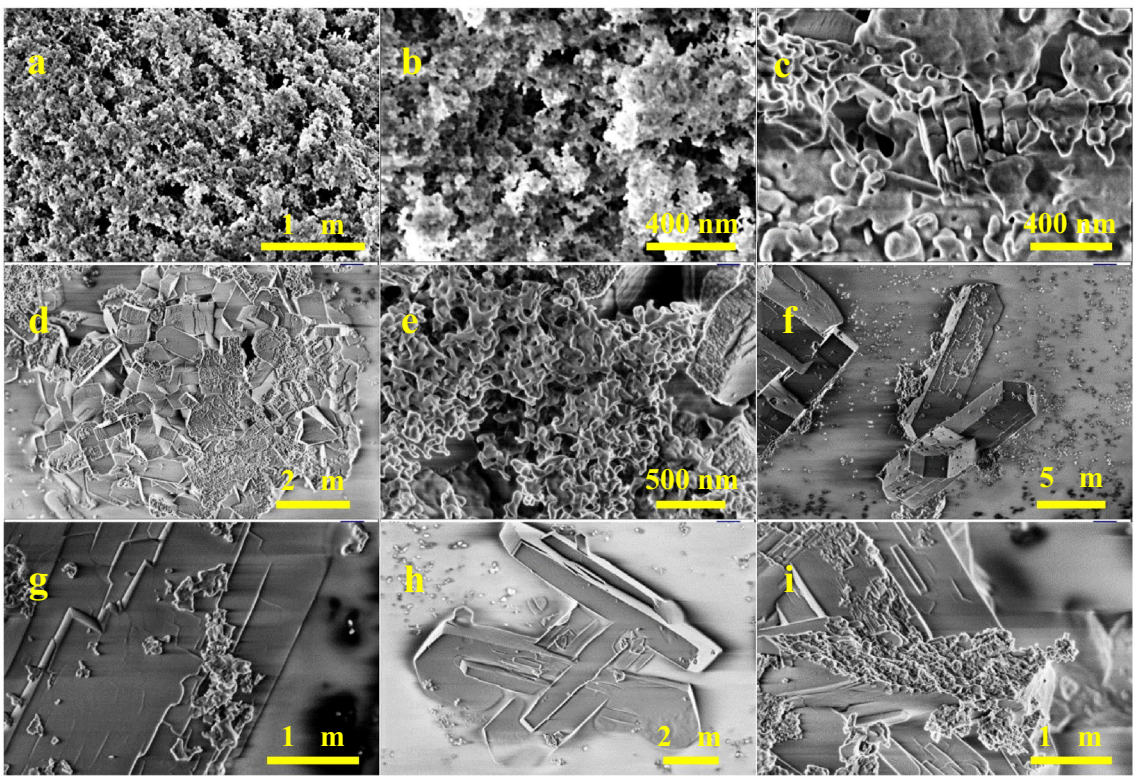

Fig. 2 Scanning electron microscopy (SEM) images of nano-SiO_2 material (**a**) and (**b**) and samples crystallized at 180 °C for (**c**) 24 h, (**d**) and (**e**) 48 h, (**f**) and (**g**) 72 h, and (**h**) and (**i**) 96 h

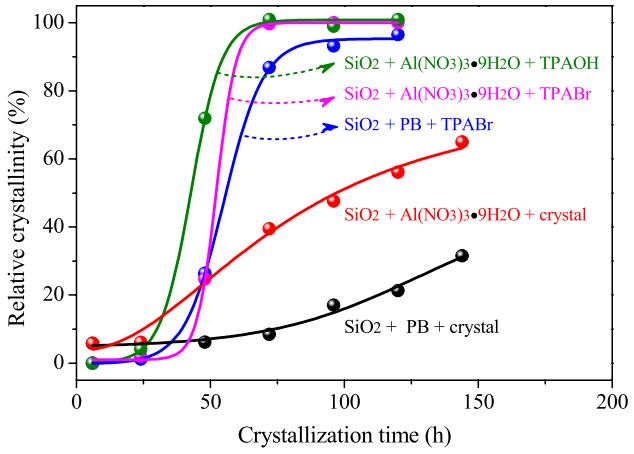

Fig. 3 The relative crystallinity kinetics of the samples synthesized with different synthetic raw materials and fixed chemical compositions at 100 SiO_2:1.0 Al_2O_3:5.5 TPAOH (or 16TPABr):25 NH_3·H_2O. Commercial nanosized ZSM-5 with SiO_2/Al_2O_3 (50) was used as the crystal seed, and its adding amount was 5 wt% based on the final product. SiO_2 and PB represent fumed silica and pseudoboehmite, respectively

materials (Fig. 4a). The crystallinity practically reached 100% after crystallization for 6 h, as shown in Fig. 4b; it required a considerably shorter crystallization time, compared with that by SAC. Figure 4c illustrates the crystallization evolution of the samples from amorphous aluminosilicate to crystallized zeolites with the increased intensity of framework Si–O–Si and Si–O–Al groups. During the DAC, PB functioned as an aluminum source and exhibited four- and six-coordinated Al species with chemical shifts at 56.6 and approximately 0 ppm, respectively, in the ^{27}Al NMR spectra (Fig. 4d). When the crystallization proceeded from 0.16 to 0.5 h, the percentage of the four-coordinated Al species decreased, while the percentage of the six-coordinated Al species increased, indicating the transformation of the four-coordinated Al species to six-coordinated derivatives. Two bands at 9.3 and 2.9 ppm demonstrated the existence of two types of six-coordinated Al species [29, 30]. Further crystallization contributed to the transformation of the Al species into the framework of ZSM-5 zeolites by dissolution, migration, nucleation, crystal growth, or direct solid-phase transformation. Thus, the amount of framework Al gradually increased with a prolonged crystallization time.

Fig. 4 **a** X-ray diffraction patterns, **b** crystallinity, **c** Fourier transform infrared (FT-IR) spectra, and **d** ^{27}Al magic-angle spinning nuclear magnetic resonance (MAS NMR) spectra of the ZSM-5 zeolites synthesized for different durations. Pseudoboehmite was used as an aluminum source, and the synthesis compositions were 100 SiO_2:1.0 Al_2O_3:5.5 TPAOH:25 NH_3·H_2O:6000 H_2O.

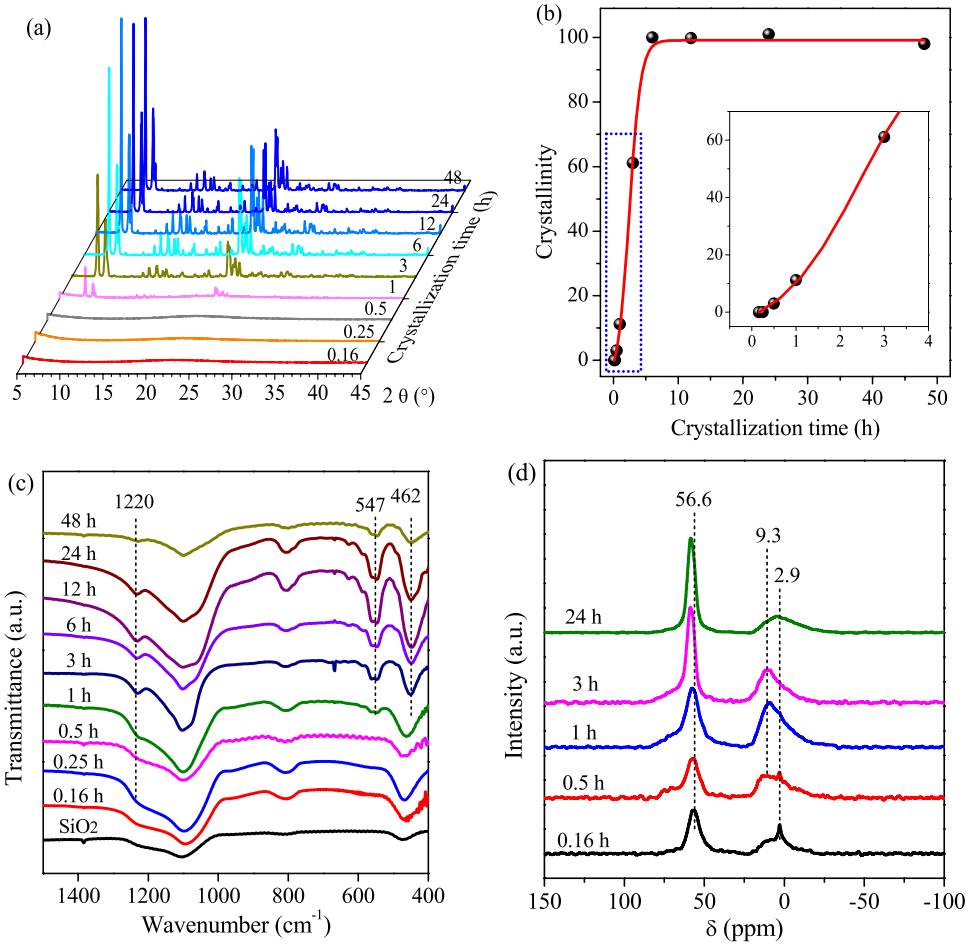

The morphologies of the samples crystallized for different durations were characterized by SEM and are shown in Fig. 5. When the crystallization proceeded to 0.25 h, aggregates were generated from the nanosilica and PB (Fig. 5b). These aggregates were transformed into aluminosilicate composites embedded with newly formed crystal nuclei. ZSM-5 zeolites wrapped with amorphous aluminosilicates appeared after a 1-h crystallization (Fig. 5d and e). With prolonged crystallization time, the amorphous aluminosilicates were gradually consumed, and clean cake-like ZSM-5 was generated (Fig. 5f–h). However, further crystallization induced surface roughening of the ZSM-5 crystallites and eventually established crosslinked crystallites with unevenly distributed size and coarse surface (Fig. 5j–l).

During the DAC process, the mass transfer of silicon and aluminum species was considerably faster than that in the SAC process, which explained the shorter time required to obtain a well-crystallized ZSM-5 zeolite when DAC was employed, as shown in Figs. 3 and 4. The crystallization evolution of amorphous aluminosilicates and crystallites, as shown in Figs. 2 and 5 demonstrated that a solid-phase transformation mechanism played a major role in converting the Si and Al sources into crystallites regardless of the method used. As shown in Fig. 6, the monomer and oligomers of the Si and Al sources could directly turn into aggregates or nanocrystallites in the presence of a structure-directing template (TPA^+ cations). The monomer, oligomers, and aggregates continuously adsorbed on the crystal surface and gradually transformed into a new crystallized surface through solid-state phase transformation [28, 31, 32]. However, the liquid-phase transformation was inevitable in the DAC process in which the Si and Al sources on the crystal surface were dissolved, adsorbed, and recrystallized on other crystal surfaces. This is why

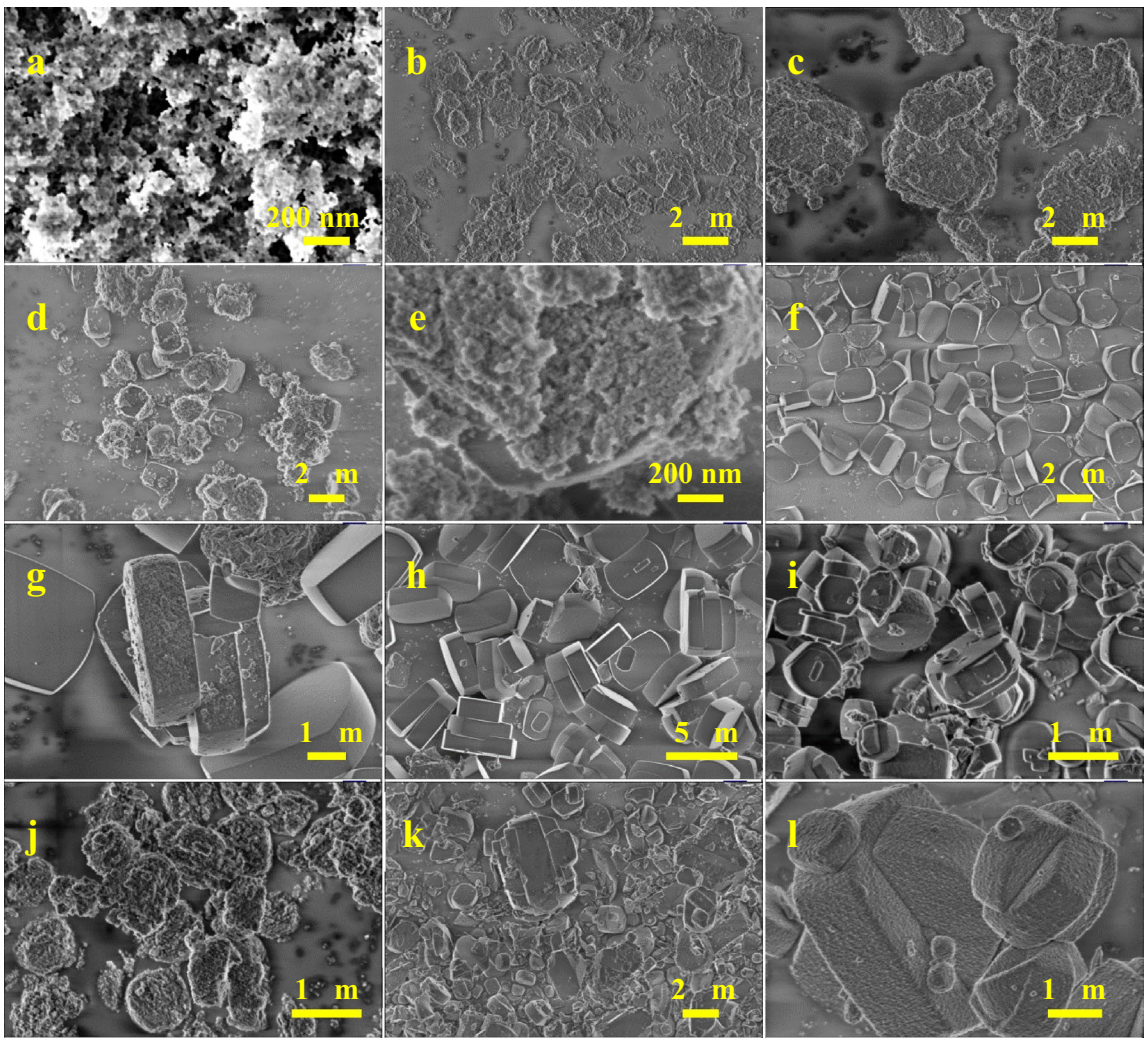

Fig. 5 Scanning electron micrograph images of (**a**) nano-SiO_2 material and samples crystallized at 180 °C for (**b**) 0.25 h, (**c**) 0.5 h, (**d**) and (**e**) 1 h, (**f**) and (**g**) 3 h, (**h**) 6 h, (**i**) 12 h, (**j**) 24 h, and (**k**) and (**l**) 48 h

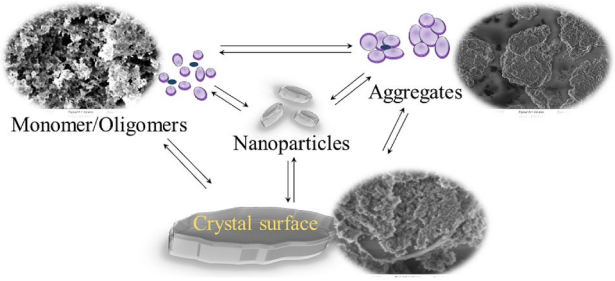

Fig. 6 Possible crystallization process for converting solid-state silica and pseudoboehmite to zeolite

uniform crystals were transformed into nonuniform crystals with prolonged crystallization time.

For comparison, the physicochemical properties of selected zeolites prepared using the two methods were characterized by N_2 sorption, NH_3-TPD, and ^{27}Al MAS NMR analysis, as shown in Fig. 7. It showed that the samples prepared by SAC and DAC for 6 h [SAC-100 and DAC-100 (6 h)] exhibited a dual-pore structure. DAC-100 (6 h) possessed higher proportional extraframework Al species but possessed a lower acid amount, compared with that prepared for 48 h [DAC-100 (48 h)]. With an increase in the crystallization time, more Al atoms were inserted into the framework of zeolite, leading to a decrease of framework SiO_2/Al_2O_3 ratio, as show in Fig. S3 and Table S1. With an increase in the SiO_2/Al_2O_3 ratios, the acid amounts of the samples prepared by SAC gradually decreased. Notably, SAC-100 and DAC-100 (48 h) virtually possessed the same number of acid sites (Table S1), demonstrating that DAC and SAC were beneficial for the synthesis of HZSM-5 zeolites.

3.3 Coupling reaction of n-heptane and methanol to light olefins

Figures 8 and 9 show the catalytic performances of n-heptane cracking and methanol conversion over SAC-100 and DAC-100. Two catalysts were crystallized with the same synthesis SiO_2/Al_2O_3 ratios of 100. Figure 8 shows that the conversions of n-heptane gradually increased with an

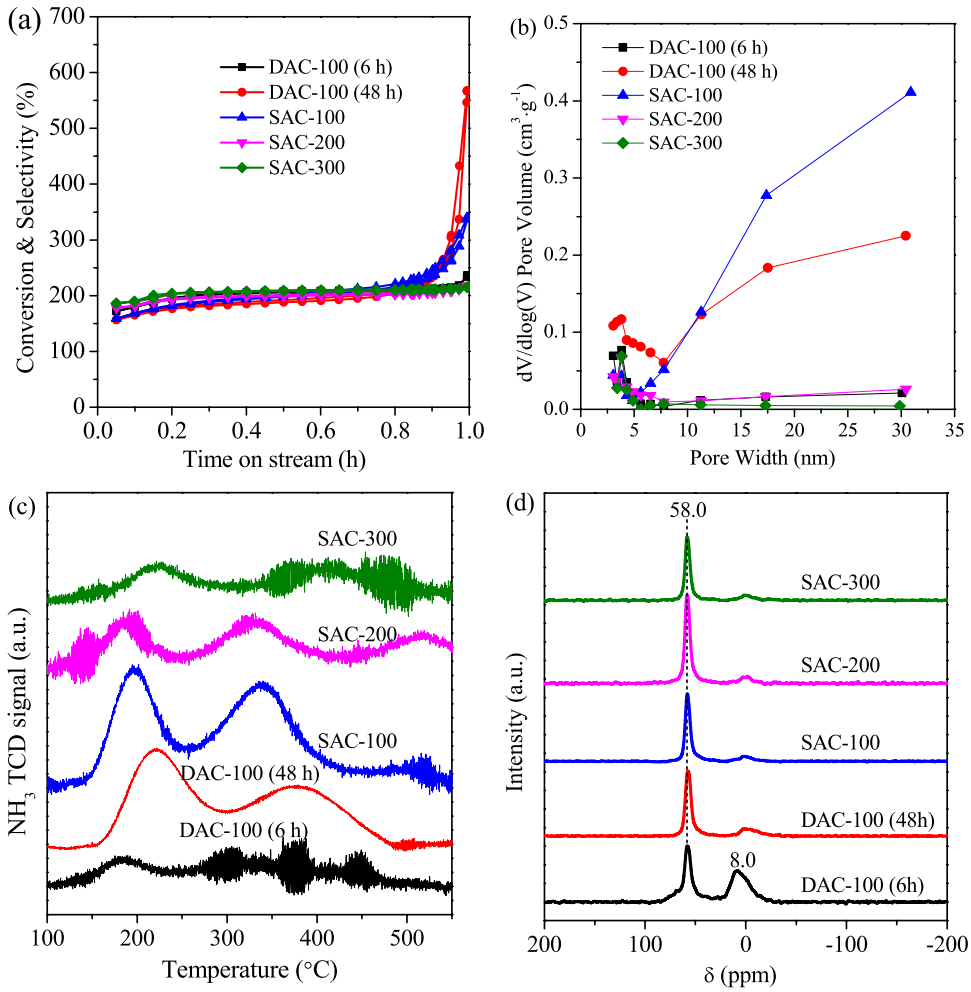

Fig. 7 N_2 sorption isotherms (**a**), Barrett–Joyner–Halenda (BJH) pore size distribution plots (**b**), ^{27}Al magic-angle spinning nuclear magnetic resonance (MAS NMR) spectra (**c**), and NH_3-TPD curves (**d**) of the selected ZSM-5 zeolites

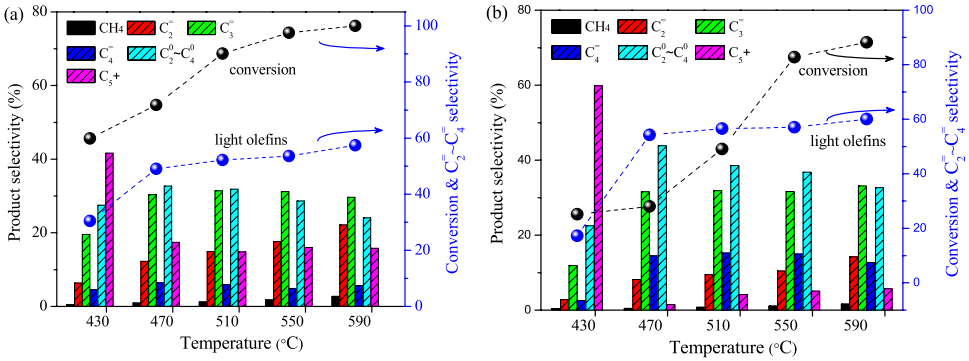

Fig. 8 Catalytic performance of n-heptane cracking over SAC-100 (**a**) and DAC-100 (**b**) catalysts at different temperatures. Reaction conditions: 1 atm and 0.1 g of the catalyst, weight hourly space velocity (WHSV) of n-heptane = 3.4 h^{-1}

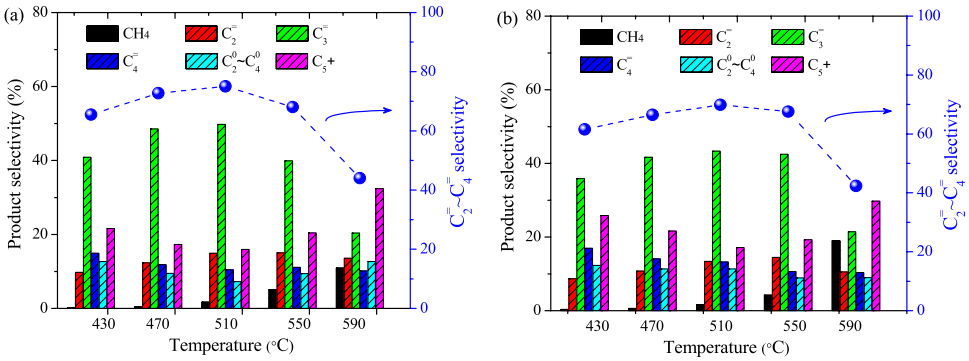

Fig. 9 Catalytic performance during the methanol to olefins (MTO) reaction over SAC-100 (**a**) and DAC-100 (**b**) catalysts at different temperatures. Reaction conditions: 1 atm and 0.1 g of the catalyst, weight hourly space volume (WHSV) of methanol = 4.0 h^{-1}

increase in the reaction temperature, and SAC-100 had a relatively higher conversion than DAC-100 at the same temperature. With the increase in temperature, ethylene selectivity gradually increased while propylene and butylene selectivity increased at first and slightly fluctuated. The selectivity for light olefins ($C_2^=$–$C_4^=$) remained unchanged when the temperature was higher than 470 °C. In contrast, the selectivity of C_5+ products except n-heptane exhibited a decreasing trend.

Methanol conversion was high for the two catalysts and practically remained at 100% within the scope of the experimental temperatures. As shown in Fig. 9, the selectivities for ethylene and propylene increased at first and decreased with an increase in the temperature, reaching a maximum point at 510 °C. However, the selectivity of the C_5+ products exhibited an opposite changing trend; it decreased at first and increased. The selectivity for light olefins ($C_2^=$–$C_4^=$) correspondingly reached the maximum point at 510 °C. In contrast, CH_4 selectivity remained low with an increase in the temperature and dramatically increased at 590 °C.

Figure 10, S4, and S5 show the variations in n-heptane cracking and methanol conversions on three SAC catalysts at different SiO_2/Al_2O_3 ratios at selected temperatures of 510 °C and 470 °C, respectively. It was observed that with an increase in the SiO_2/Al_2O_3 ratios, the conversion of n-heptane gradually decreased, while the selectivity for light olefins increased. Meanwhile, ethylene selectivity decreased, but propylene selectivity increased (Fig. 10a). Compared with n-heptane, methanol exhibited higher reactivity and was completely converted over three catalysts (Fig. 10b). In addition, the selectivities for propylene and light olefins during methanol conversion were considerably higher than those during n-heptane cracking. With an increase in the SiO_2/Al_2O_3 ratios, the selectivity for propylene and light olefins slightly increased, and ethylene selectivity decreased.

In comparison, ZSM-5 catalysts prepared by DAC were tested during methanol conversion (Figs. S6 and 11). The result showed that methanol was completely converted and that the catalyst lifetimes increased with an increase in crystallization time. After a short crystallization time of 1 h, the ZSM-5 catalyst was not well crystallized, and a large number of amorphous aluminosilicates remained (Fig. 5d), resulting in a short catalyst lifetime. When the catalysts were well crystallized, the Al atoms became uniformly distributed in the framework of the ZSM-5 catalysts, and their lifetimes were prolonged accordingly. However, the selectivities for propylene and light olefins increased at first and decreased. After a 48-h crystallization, the ZSM-5 catalyst exhibited the lowest propylene selectivity, probably because of its rough surface and unevenly crystal size, as shown in Fig. 5k.

Numerous studies have been conducted on the mechanisms of the conversion of methanol and alkanes [33–35]. For methanol conversion over zeolitic catalysts, the dual-cycle mechanism including olefinic- and aromatic-based

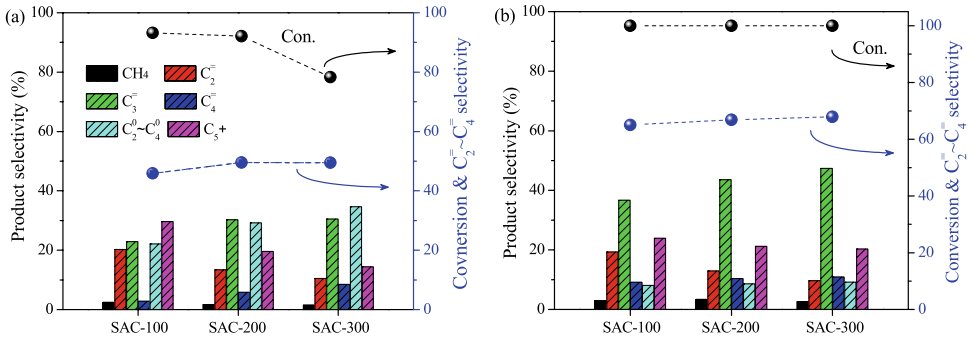

Fig. 10 Catalytic performance of the ZSM-5 catalysts at different SiO_2/Al_2O_3 ratios during the (**a**) n-heptane cracking and (**b**) methanol to olefins (MTO) reaction. Reaction conditions: 1 atm and 0.1 g of the catalyst; n-heptane cracking was conducted at 550 °C with weight hourly space volume (WHSV) = 3.4 h^{-1}, while the MTO reaction was conducted at 470 °C with WHSV = 4.0 h^{-1}.

cycles that are run simultaneously, has been widely accepted [36, 37]. As shown in Fig. 12, the olefinic- and aromatic-based cycles over the acid sites of ZSM-5 catalysts contribute to the formation of light olefins. However, propylene and higher alkenes are preferentially produced via the olefinic-based cycle from successive alkene methylation and cracking reactions. Contrarily, ethylene and aromatic species are mainly produced via the aromatic-based cycle from methylbenzenes, which undergo side-chain methylation, ring contraction, or ring expansion reactions [38, 39]. Previous studies have confirmed that the high density of acid sites contributes to the aromatic-based cycle, thereby forming more ethylene and aromatic species. A decrease in the acid density ensures a high propylene yield and catalyst lifetime via the olefinic-based cycle [19, 34, 38, 40, 41]. This correlated with the results shown in Fig. 10b that an increase in the SiO_2/Al_2O_3 ratio of SAC catalysts could increase propylene selectivity but decrease ethylene selectivity.

Compared with methanol conversion, it is widely accepted that the carbocation transition ions (carbonium ions and carbenium ions) on acid sites via protonation and/or dehydrogenation reactions are formed first on acid sites in the catalytic cracking of alkanes and then consecutive reactions, such as the break-up of C–C bonds, hydrogen transfer, oligomerization, cyclization, and aromatization occur to form a wide range of products [42–43]. As shown in Fig. 10a, the SAC catalysts with high SiO_2/Al_2O_3 ratios exhibited low acid density, resulting in high propylene selectivity by reducing the hydrogen transfer reaction of light olefins. However, the n-heptane conversion decreased if the number of acid sites or acid strength was insufficient for catalytic cracking, as shown in Figs. 4d and 7d, and S7 that poorly crystallized catalysts possessed high proportional extraframework Al species, which were generally regarded as weak acid sites [2, 44].

The coreaction of n-heptane and methanol was conducted over SAC-100 at 550 °C to investigate the interaction of the two feeds. Figure 13a shows the effects of the ratios of n-heptane to methanol on their conversions and product selectivities. Within the scope of the study, methanol was converted, while the n-heptane conversion gradually increased with a decrease in its usage, indicating that high activation energy is required for n-heptane cracking. Compared with a separate feed, the coreaction of n-heptane and methanol exhibited high selectivity for light olefins, reaching a maximum value of 54.83% at a molar ratio of 1:1, which was considerably higher than that of n-heptane alone (46.88%) and methanol alone (50.86%). It is in agreement with previous studies, in which Sun et al. [45] studied the impact of adding C_{3-6} olefins to methanol over a HZSM-5 catalysts on activity and selectivity. It was found that cofeeding small concentrations of olefins did not selectively suppress the catalytic cycle of methanol conversion based on aromatic molecules, however, it could enhance the methylation rate of olefins with increasing concentration of the co-fed olefin and produce more propene than the single pass methanol conversion. As shown in Fig. 11, the cracking of n-heptane increased the content of light olefins, such as propylene and butylene and further increased the degree of methanol involved in the olefinic-based cycle reaction, thereby improving the selectivity for light olefins [11] (see Fig. 12).

With an increase in methanol usage, the selectivities for methane and C_5+ products gradually increased, indicating that methanol tended to form aromatics at the high temperature of 550 °C. The variations of the conversion and product selectivity versus time on stream with a n-heptane to methanol molar ratio of 1 are shown in Fig. 13b and c. With an increase in reaction time, methanol was completely converted, and its conversion rapidly decreased after 18 h, while the n-heptane conversion was relatively high, and its decreasing rate was slow at first and then fast. The selectivities for light olefins and C_2^0–C_4^0 gradually decreased; however, the selectivities for methane and C_5+ products increased with an increase in reaction time, which was ascribed to the change in reaction pathways as the catalyst

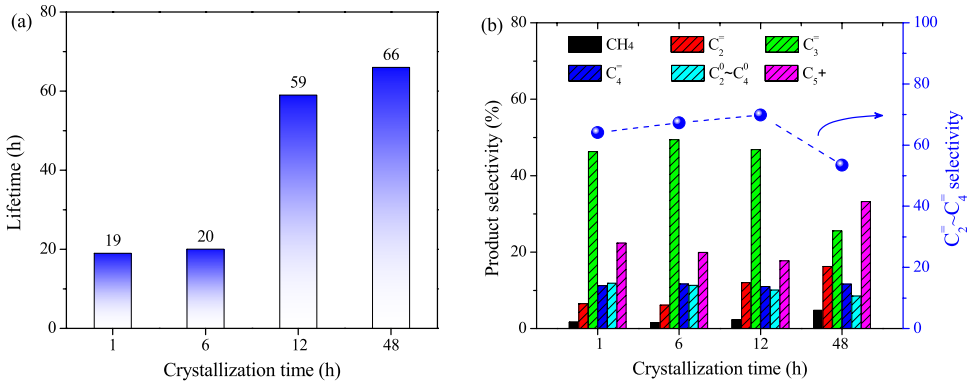

Fig. 11 Catalytic performance of the ZSM-5 catalysts during the methanol to olefins (MTO) reaction. Catalyst lifetime (**a**) and product selectivity (**b**) versus the crystallization time of the zeolites. Reaction conditions: 1 atm and 0.1 g of the catalyst, 470 °C, weight hourly space velocity (WHSV) of methanol = 4.0 h^{-1}

deactivated. Compared with the coreaction of n-heptane and methanol, the conversion of n-heptane alone was lower at the same reaction time, but the selectivities for light olefins remained relatively stable with an increase in reaction time (Fig. 13d). This demonstrates that the coreaction of n-heptane and methanol improved the cracking of n-heptane. However, a high light olefin content accelerated the oligomerization, cyclization, and aromatization reactions, which contributed to the aromatic-based cycle reactions and accelerated the deactivation due to coking [46, 47]. It is consistent with the result reported by Xue et al., in the coreaction of methanol and butene, it was found that increasing butene content leads to low propene yield due to the

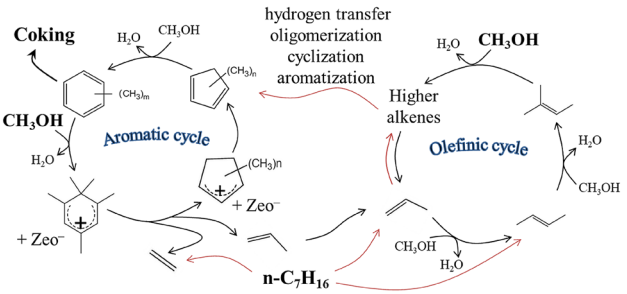

Fig. 12 Reaction pathway for the coreaction of methanol and n-heptane by a dual-cycle mechanism

Fig. 13 Average values of the conversion and product selectivity before the n-heptane conversion was lower than 85% (**a**). The variations in the conversion and product selectivity versus time on stream with a n-heptane to methanol molar ratio of 1 (**b**) and (**c**). The catalytic performance of a separate feed of n-heptane (**d**). Reaction conditions; 0.10 g of SAC-100, 1 atm, and 550 °C

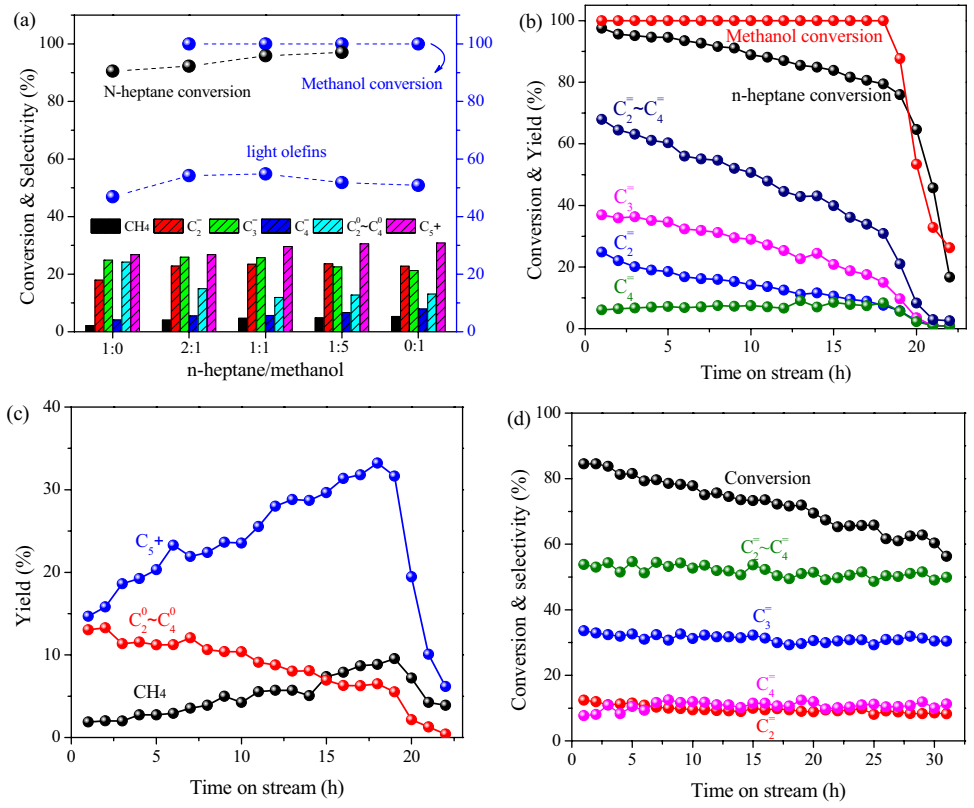

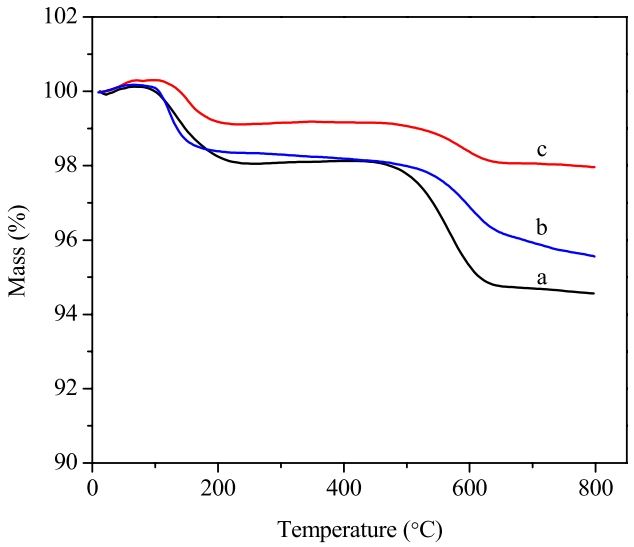

Fig. 14 Weight loss of spent SAC-100 catalysts by the **a** coreaction of methanol, **b** n-heptane alone, and **c** methanol alone

enhancement of the dimerization-cracking of olefins, and methanol/butene molar ratio of 4:1 was optimum for producing propylene [10]. The coking properties of the spent catalysts with different feedings were characterized by TGA and are shown in Fig. 14. This showed that the catalyst using methanol and n-heptane as a mixed feed had the biggest amount of coke, indicating an enhanced aromatic-based cycle reaction.

4 Conclusion

Here, H-form ZSM-5 zeolites were directly synthesized by SAC and DAC using ammonia hydroxide as a mineralizer and solid fumed silica and PB as raw materials. The evolution of the crystallization process demonstrates that the solid-phase transformation mechanism plays a major role in converting silicon and aluminum sources into crystallites regardless of the method used. In addition, the mass transfer of Si and Al sources is crucial for crystallization, and the crystallization rate of HZSM-5 by DAC is significantly faster than that by SAC. The coreaction of n-heptane and methanol over the HZSM-5 catalyst improved the cracking of n-heptane, which exhibited high selectivity for light olefins but a faster deactivation rate, compared with that from separate feeds.

Supplementary Information The online version contains supplementary material available at https://doi.org/10.1007/s10934-022-01359-2.

Acknowledgements This work was supported by the National Natural Science Foundation of China (No. 21908240), Natural Science Foundation of Jiangsu Province (No. BK20190625), PetroChina Innovation Foundation (No. 2020D-5007-0403), and the Priority Academic Program Development of Jiangsu Higher Education Institutions.

Author contributions RF & MZ (conceptualization, supervision, data analysis and manuscript writing), BL (experimentation, data analysis and drafting of manuscript), XH (data analysis), XY (experimentation and data analysis). All authors have given approval to the final version of the manuscript.

Declarations

Conflict of interest There are no conflicts of interest to declare.

References

1. P. del Campo, C. Martínez, A. Corma, Activation and conversion of alkanes in the confined space of zeolite-type materials. Chem. Soc. Rev. **50**, 8511–8595 (2021)
2. X. Xiao, B. Sun, P. Wang, X. Fan, L. Kong, Z. Xie, B. Liu, Z. Zhao, Tuning the density of Brønsted acid sites on mesoporous ZSM-5 zeolite for enhancing light olefins selectivity in the catalytic cracking of n-octane. Microporous Mesoporous Mater. **330**, 111621 (2022)
3. P. Tian, Y. Wei, M. Ye, Z. Liu, Methanol to Olefins (MTO): From Fundamentals to Commercialization. ACS Catal. **5**, 1922–1938 (2015)
4. X. Sun, S. Mueller, Y. Liu, H. Shi, G.L. Haller, M. Sanchez-Sanchez, A.C. van Veen, J.A. Lercher, On reaction pathways in the conversion of methanol to hydrocarbons on HZSM-5. J. Catal. **317**, 185–197 (2014)
5. W. Wu, W. Guo, W. Xiao, M. Luo, Methanol conversion to olefins (MTO) over H-ZSM-5: Evidence of product distribution governed by methanol conversion. Fuel Process. Technol. **108**, 19–24 (2013)
6. M. Khanmohammadi, S. Amani, A.B. Garmarudi, A. Niaei, Methanol-to-propylene process: Perspective of the most important catalysts and their behavior. Chin. J. Catal. **37**, 325–339 (2016)
7. R. Feng, X. Yan, X. Hu, Y. Zhang, J. Wu, Z. Yan, The effect of co-feeding ethanol on a methanol to propylene (MTP) reaction over a commercial MTP catalyst. Appl. Catal. A **592**, 117429 (2020)
8. H. Koempel, W. Liebner, Lurgi's methanol to propylene (MTP®) report on a successful commercialisation. Stud. Surf. Sci. Catal. **167**, 261–267 (2007)
9. J. Valecillos, E. Epelde, J. Albo, A.T. Aguayo, J. Bilbao, P. Castaño, Slowing down the deactivation of H-ZSM-5 zeolite catalyst in the methanol-to-olefin (MTO) reaction by P or Zn modifications. Catal. Today **348**, 243–256 (2020)
10. Y. Xue, J. Li, S. Wang, X. Cui, M. Dong, G. Wang, Z. Qin, J. Wang, W. Fan, Co-reaction of methanol with butene over a high-silica H-ZSM-5 catalyst. J. Catal. **367**, 315–325 (2018)
11. E. Ebadzadeh, M.H. Khademi, M. Beheshti, A kinetic model for methanol-to-propylene process in the presence of co-feeding of C4-C5 olefin mixture over H-ZSM-5 catalyst. Chem. Eng. J. **405**, 126605 (2021)
12. T. Liang, J. Chen, Z. Qin, J. Li, P. Wang, S. Wang, G. Wang, M. Dong, W. Fan, J. Wang, Conversion of methanol to olefins over H-ZSM-5 zeolite: Reaction pathway is related to the framework aluminum siting. ACS Catal. **6**, 7311–7325 (2016)
13. J. Zhong, J. Han, Y. Wei, Z. Liu, Catalysts and shape selective catalysis in the methanol-to-olefin (MTO) reaction. J. Catal. **396**, 23–31 (2021)

14. A. Javdani, J. Ahmadpour, F. Yaripour, Nano-sized ZSM-5 zeolite synthesized via seeding technique for methanol conversions: A review. Microporous Mesoporous Mater. **284**, 443–458 (2019)
15. D.M. Bibby, N.B. Milestone, L.P. Aldridge, NH_4^+-tetraalkyl ammonium systems in the synthesis of zeolites. Nature **285**, 30–31 (1980)
16. D. Wu, X. Yu, X. Chen, G. Yu, K. Zhang, M. Qiu, W. Xue, C. Yang, Z. Liu, Y. Sun, Morphology-controlled synthesis of H-type MFI zeolites with unique stacked structures through a one-pot solvent-free strategy. ChemSusChem **12**, 3871–3877 (2019)
17. H. Shen, M. Liu, J. Li, X. Li, S. Xie, F. Chen, L. Xu, X. Guo, C. Song, X. Zhu, Promising strategy to synthesize ZSM-5@Silicalite-1 with superior catalytic performance for catalytic cracking reactions. Ind. Eng. Chem. Res. **60**, 9098–9106 (2021)
18. Z. Hou, X. Mi, X. Li, H. Liu, Seed-assisted aynthesis of ZSM-5 aggregates assembled from regularly stacked nanosheets and their performance in n-hexane aromatization. Ind. Eng. Chem. Res. **60**, 12100–12108 (2021)
19. R. Feng, X. Yan, X. Hu, Y. Zhang, J. Wu, Z. Yan, Phosphorus-modified b-axis oriented hierarchical ZSM-5 zeolites for enhancing catalytic performance in a methanol to propylene reaction. Appl. Catal. A **594**, 117464 (2020)
20. R. Feng, X. Yan, X. Hu, J. Wu, Z. Yan, Direct synthesis of b-axis oriented H-form ZSM-5 zeolites with an enhanced performance in the methanol to propylene reaction. Microporous Mesoporous Mater. **302**, 110246 (2020)
21. Y. Wang, T. Li, C. Li, J. Lu, C. Dai, F. Subhan, P. Bai, H. Sun, R. Feng, Z. Yan, One-pot green synthesis of Fe-ZSM-5 zeolite containing framework heteroatoms via dry gel conversion for enhanced propylene selectivity of catalytic cracking catalyst. J. Mater. Sci. **56**, 18050–18060 (2021)
22. J. Zhou, J. Teng, L. Ren, Y. Wang, Z. Liu, W. Liu, W. Yang, Z. Xie, Full-crystalline hierarchical monolithic ZSM-5 zeolites as superiorly active and long-lived practical catalysts in methanol-to-hydrocarbons reaction. J. Catal. **340**, 166–176 (2016)
23. R. Feng, X. Yan, X. Hu, Y. Wang, Z. Li, K. Hou, J. Lin, Hierarchical ZSM-5 zeolite designed by combining desilication and dealumination with related study of n-heptane cracking performance. J. Porous Mater. **25**, 1743–1756 (2018)
24. S.K. Jesudoss, J.J. Vijaya, K. Kaviyarasu, L.J. Kennedy, R. Jothi Ramalingam, H. A. Al-Lohedan, Anti-cancer activity of hierarchical ZSM-5 zeolites synthesized from rice-based waste materials. RSC Adv. **8**, 481–490 (2018)
25. S.M. Al-Jubouri, Synthesis of hierarchically porous ZSM-5 zeolite by self-assembly induced by aging in the absence of seeding-assistance. Microporous Mesoporous Mater. **303**, 110296 (2020)
26. T. Imyen, W. Wannapakdee, S. Ittisanronnachai, T. Witoon, C. Wattanakit, Tailoring hierarchical zeolite composites with two distinct frameworks for fine-tuning the product distribution in benzene alkylation with ethanol. Nanoscale Adv. **2**, 4437–4449 (2020)
27. R. Feng, X. Wang, J. Lin, Z. Li, K. Hou, X. Yan, X. Hu, Z. Yan, M.J. Rood, Two-stage glucose-assisted crystallization of ZSM-5 to improve methanol to propylene (MTP). Microporous Mesoporous Mater. **270**, 57–66 (2018)
28. Y. Wang, J. Song, N.C. Baxter, G.-T. Kuo, S. Wang, Synthesis of hierarchical ZSM-5 zeolites by solid-state crystallization and their catalytic properties. J. Catal. **349**, 53–65 (2017)
29. S. Dong, W. Shi, J. Zhang, S. Bi, 27Al NMR Chemical Shifts and Relative Stabilities of Aqueous Monomeric Al3 + Hydrolytic Species with Different Coordination Structures. ACS Earth Space Chem. **3**, 1353–1361 (2019)
30. M. Haouas, F. Taulelle, C. Martineau, Recent advances in application of ^{27}Al NMR spectroscopy to materials science. Prog Nucl. Magn. Reson. Spectrosc. **94–95**, 11–36 (2016)
31. N. Ren, B. Subotić, J. Bronić, Y. Tang, M. Dutour Sikirić, T. Mišić, V. Svetličić, S. Bosnar, T. Antonić Jelić, Unusual pathway of crystallization of zeolite ZSM-5 in a heterogeneous system: Phenomenology and starting considerations. Chem. Mater. **24**, 1726–1737 (2012)
32. M.H. Do, T. Wang, D. Cheng, F. Chen, X. Zhan, J. Gong, Zeolite growth by synergy between solution-mediated and solid-phase transformations. J. Mater. Chem. A **2**, 14360–14370 (2014)
33. L. Palumbo, F. Bonino, P. Beato, M. Bjørgen, A. Zecchina, S. Bordiga, Conversion of methanol to hydrocarbons: Spectroscopic characterization of carbonaceous species formed over H-ZSM-5. J. Phys. Chem. C **112**, 9710–9716 (2008)
34. M. Bjørgen, S. Svelle, F. Joensen, J. Nerlov, S. Kolboe, F. Bonino, L. Palumbo, S. Bordiga, U. Olsbye, Conversion of methanol to hydrocarbons over zeolite H-ZSM-5: On the origin of the olefinic species. J. Catal. **249**, 195–207 (2007)
35. S. Ilias, A. Bhan, Mechanism of the catalytic conversion of methanol to hydrocarbons. ACS Catal. **3**, 18–31 (2013)
36. S. Wang, Y. Chen, Z. Wei, Z. Qin, J. Chen, H. Ma, M. Dong, J. Li, W. Fan, J. Wang, Theoretical insights into the mechanism of olefin elimination in the methanol-to-olefin process over HZSM-5, HMOR, HBEA, and HMCM-22 zeolites. J. Phys. Chem. A **118**, 8901–8910 (2014)
37. Z. Wei, Y.-Y. Chen, J. Li, W. Guo, S. Wang, M. Dong, Z. Qin, J. Wang, H. Jiao, W. Fan, Stability and reactivity of intermediates of methanol related reactions and C–C bond formation over H-ZSM-5 acidic catalyst: A computational analysis. J. Phys. Chem. C **120**, 6075–6087 (2016)
38. R. Feng, B. Liu, P. Zhou, X. Yan, X. Hu, M. Zhou, Z. Yan, Influence of framework Al distribution in HZSM-5 channels on catalytic performance in the methanol to propylene reaction. Appl. Catal. A **629**, 118422 (2022)
39. E.D. Hernandez, B. Manookian, S.M. Auerbach, F.C. Jentoft, Shape-selective synthesis of alkylcyclopentenyl cations in zeolites and spectroscopic distinction of constitutional isomers. ACS Catal. **11**, 12893–12914 (2021)
40. X. Huang, H. Li, H. Li, W.-D. Xiao, Modeling and analysis of the Lurgi-type methanol to propylene process: Optimization of olefin recycle. AlChE J. **63**, 306–313 (2017)
41. S. Kotrel, H. Knözinger, B.C. Gates, The Haag-Dessau mechanism of protolytic cracking of alkanes. Microporous Mesoporous Mater. **35–36**, 11–20 (2000)
42. K.A. Cumming, B.W. Wojciechowski, Hydrogen transfer, coke formation, and catalyst decay and their role in the chain mechanism of catalytic cracking. Catal. Rev. **38**, 101–157 (1996)
43. J. Wang, J. Shan, Y. Tian, T. Zhu, H. Duan, X. He, C. Qiao, G. Liu, Catalytic cracking of n-heptane over Fe modified HZSM-5 nanosheet to produce light olefins. Fuel **306**, 121725 (2021)
44. C. Wang, Y. Chu, J. Xu, Q. Wang, G. Qi, P. Gao, X. Zhou, F. Deng, Extra-framework aluminum-assisted initial C – C bond formation in methanol-to-olefins conversion on zeolite H-ZSM-5. Angew Chem. Int. Ed. **57**, 10197–10201 (2018)
45. X. Sun, S. Mueller, H. Shi, G.L. Haller, M. Sanchez-Sanchez, A.C. van Veen, J.A. Lercher, On the impact of co-feeding aromatics and olefins for the methanol-to-olefins reaction on HZSM-5. J. Catal. **314**, 21–31 (2014)
46. I. Pinilla-Herrero, E. Borfecchia, T. Cordero-Lanzac, U.V. Mentzel, F. Joensen, K.A. Lomachenko, S. Bordiga, U. Olsbye, P. Beato, S. Svelle, Finding the active species: The conversion of methanol to aromatics over Zn-ZSM-5/alumina shaped catalysts. J. Catal. **394**, 416–428 (2021)
47. J. Zhang, Z. Huang, L. Xu, X. Zhang, X. Zhang, Y. Yuan, L. Xu, Verifying the olefin formation mechanism of the methanol-to-hydrocarbons reaction over H-ZSM-48. Catal. Sci. Technol. **9**, 2132–2143 (2019)